

Review

The Higgs Mechanism and Spacetime Symmetry

Irina Dymnikova

A.F. Ioffe Physico-Technical Institute of the Russian Academy of Sciences, Polytekhnicheskaja 26, 194021 St. Petersburg, Russia; igd.amp@mail.ioffe.ru or irina@uwm.edu.pl; Tel.: +7-812-292-7912

Received: 29 August 2020; Accepted: 12 October 2020; Published: 15 October 2020



Abstract: In this review, we summarize the results of the analysis of the inherent relation between the Higgs mechanism and spacetime symmetry provided by generic incorporation of the de Sitter vacuum as a false vacuum with the equation of state $p = -\rho$. This relation has been verified by the application for the interpretation of the experimental results on the negative mass squares for neutrinos, and of the appearance of the minimal length in the annihilation reaction $e^+e^- \rightarrow \gamma\gamma(\gamma)$. An additional verification is expected for the dark matter candidates with the interior de Sitter vacuum of the GUT scale, whose predicted observational signatures include the induced proton decay in the matter of an underground detector, such as IceCUBE.

Keywords: higgs mechanism; de Sitter vacuum; spacetime symmetry

1. Introduction

The Higgs mechanism generically involves the de Sitter vacuum as the false vacuum state of its scalar field(s) with $p = -\rho$. As a result, mass generation involves gravity produced by the de Sitter vacuum and the related de Sitter spacetime symmetry. The spontaneous symmetry breaking of scalar fields leads then to breaking of spacetime symmetry from the de Sitter group in the gravito-electroweak vertex to the Poincaré group in the region of a distant observer [1].

In the current literature, the relation between mass and the symmetry of spacetime has been considered in the context of the Lorentz symmetry breaking [2], and in the alternative Higgs-like mechanism for mass generation [3]. The relation of mass with gravity has been considered in the framework of the ratio gravity, in which the gravitational interaction is considered not as a universal interaction corresponding to a curved spacetime, but on an equal footing with other fields in the flat spacetime [4,5], and lepton and quark masses originate from the relevant SU2 algebras of gauge transformation [6] (for more details, see [1]).

In General Relativity, the mass of a regular object with de Sitter vacuum interior is generically related with the breaking of spacetime symmetry from the de Sitter group in its origin [7] (for a review, see [1]).

The inherent relation of the Higgs mechanism with the spacetime symmetry can be verified by analysis of the experimental data on negative mass squares for neutrino obtained since 1991 [8]. Proposed in the literature are explanations involving the hypothesis that neutrinos are superluminal fermions [9], a new theory of a mass as a dynamical variable [10], and an approach with an additional charged current, more than an order of magnitude weaker than that in the standard model [11]. In our analysis [12,13], we take into account that the interaction vertex should have to be gravito-electroweak due to intrinsic involvement of gravity of the de Sitter vacuum, and apply the Casimir operators in the de Sitter space for description of particle states in the vertex. This allows us to shed some light on the origin of the negative mass squares and to evaluate a scale of the gravito-electroweak unification from the currently reported experimental results on negative mass squares [13].

Another observational case applied for analysis of essential involvement of gravity in the Higgs mechanism is revealing with the 5σ significance of the minimal length $l_e = 1.57 \times 10^{-17}$ cm

in the annihilation reaction $e^+e^- \rightarrow \gamma\gamma(\gamma)$ at the energy $E = 1.253 \text{ TeV}$ [14,15]. For analysis of this reaction, we have to apply an approach involving some model of an extended electron, because in this case both its classical radius $r_e = e^2/(m_e c^2) = 2.8 \times 10^{-13} \text{ cm}$ and the Compton wavelength $\lambda_e = \hbar/(m_e c) = 3.9 \times 10^{-11} \text{ cm}$ exceed substantially the test distances characterized by $l_e = 1.57 \times 10^{-17} \text{ cm}$. The general approach is provided by Nonlinear Electrodynamics Coupled to Gravity (NED-GR), which admit the class of regular solutions describing electrically charged spinning electromagnetic solitons with the de Sitter vacuum interior and the gyromagnetic ratio $g = 2$ for a distant observer [16,17] (for a review, see [18]).

Solitons are defined as the Coleman lumps, regular particle-like non-dissipative self-gravitating objects [19]. NED-GR solitons are governed by the electromagnetic and gravitational self-interaction.

Electrically neutral solitons with the de Sitter interiors [20] are guided by the Einstein equations, related by the gravitational interaction and for this reason called G-lumps [7]. They are described by the regular solutions which belong to the Kerr–Schild class [21]. The source terms in the Einstein equations are presented by stress–energy tensors with the algebraic structure such that [7,22]

$$T_t^t = T_r^r \quad (p_r = -\rho). \tag{1}$$

The transversal pressure is related to the density as $p_\perp = -\rho - r\rho'/2$.

Stress–energy tensors evolve from the de Sitter vacuum in the origin $T_k^i = \rho_\Lambda \delta_k^i$ to the Minkowski vacuum $T_k^i = 0$ in the asymptotically flat spacetime, either to the de Sitter vacuum $T_k^i = \rho_\lambda \delta_k^i$ with $\lambda < \Lambda$, in the spacetime with two vacuum scales, $\rho_\Lambda = (8\pi G)^{-1}\Lambda$, $\rho_\lambda = (8\pi G)^{-1}\lambda$.

The Kerr–Schild metric in the Schwarzschild coordinates reads

$$ds^2 = g(r)dt^2 - \frac{dr^2}{g(r)} - r^2 d\Omega^2; \quad g(r) = 1 - \frac{2G}{r} \mathcal{M}(r); \quad \mathcal{M}(r) = \int_0^r \rho(x)x^2 dx \tag{2}$$

where $d\Omega^2 = r^2(d\theta^2 + \sin^2\theta d\phi^2)$.

The number of spacetime horizons is constrained by $N_{horizons} \leq (2N_{vacuum\ scales} - 1)$ [23]. In the asymptotically flat spacetime with the de Sitter center, which we overview below, $N_{horizons} \leq 2$, and compact objects with the de Sitter vacuum interiors are presented by regular black (white) holes with the event and internal horizons, G-lumps without horizons, and the extreme black hole states with the double horizons, which are the stable remnants of the black hole evaporation (for a review, see [24]).

Regular black hole remnants and G-lumps can be considered as heavy Dark Matter (DM) candidates ([25] and references therein), whose observational signatures depend essentially on the energy scale of the internal de Sitter vacuum.

For G-lumps and regular black hole remnants with the GUT scale interiors, the observational signature has been predicted conditioned by non-conservation of the baryon and lepton numbers, which may lead to an induced proton decay in the matter of an underground detector [26]. It can be important for supergravity unified models in which the lifetime of the proton is found sensitive to the mass of the Higgs boson [27].

In Section 2, we outline the analysis of negative mass squares for neutrino. Section 3 presents the results of analysis of the origin of the minimal length in the annihilation reaction $e^+e^- \rightarrow \gamma\gamma(\gamma)$ with applying the basic properties of the spinning electromagnetic soliton. In Section 4, we overview the basic properties and observational signatures of the heavy DM candidates with the de Sitter vacuum interiors, and Section 5 contains the conclusions.

2. Negative Mass Squares for Neutrino

The results on the negative mass squares for neutrino reported first in 1991 [8] were summarized by the Particle Data Group in 1994 to the average value $m_\nu^2 = -54 \pm 30 \text{ eV}^2/c^4$, qualified as anomalous due to a shift to the unphysical region [28]. In 1995, the Lawrence Livermore National Laboratory reported

the results of the experiment on neutrino mass searches in tritium β -decay, fitted, with the improved accuracy, to a squared mass of $m^2(\nu_e) = (-120 \pm 20) \text{ eV}^2$ [29]. The problem with the unphysical negative value of m^2 appeared also in this case despite the relatively small errors, suggesting some unrecognised systematic error sources responsible for this effect. The values for the mass squares allow to derive the limits on the neutrino masses. The existing experimental and cosmological neutrino data constrain the heaviest neutrino mass m_3 within the range $5 \times 10^{-2} \text{ eV} \simeq \sqrt{\Delta m_A^2} \leq m_3 \leq \frac{1}{3} \sum_i m_i \simeq 3 \times 10^{-1} \text{ eV}$ where $\Delta m_A^2 = \Delta m_{23}^2 = m_3^2 - m_2^2 \simeq 2.5 \times 10^{-3} \text{ eV}^2$ is the atmospheric neutrino mass square difference [30].

The recent results of the Karlsruhe Tritium Neutrino experiment KATRIN gives the best fit for an effective mass square value $m_\nu^2 = (-1.0_{-1.1}^{+0.9}) \text{ eV}^2$ corresponding to a 1σ statistical fluctuation to negative values of m_ν^2 with $p = 0.16$. The total uncertainty is dominated by $\sigma_{stat}^2 (0.97 \text{ eV}^2)$ versus $\sigma_{syst}^2 (0.32 \text{ eV}^2)$ [31]. From this value, an upper limit 1.1 eV is derived at the 90% confidence level on the absolute mass scale of neutrinos [31], represented by the effective neutrino mass $m_\beta = \sqrt{|U_{e1}|^2 m_1^2 + |U_{e2}|^2 m_2^2 + |U_{e3}|^2 m_3^2}$, where U_{ei} is the leptonic flavor mixing matrix and m_i are the absolute neutrino masses; the limit $m_\beta < 1.1 \text{ eV}$ is for now the most stringent upper limit ([32] and references therein). (For a comprehensive review on the search for neutrino masses, see [30,32–34].)

Here we consider a possible origin of negative mass squares provided by spacetime symmetry. The basic feature of the Higgs mechanism is the spontaneous symmetry breaking of the intrinsically involved scalar fields from the false vacuum state $p = -\rho$ to the true vacuum state $p = \rho = 0$. The key point is that a false vacuum with the equation of state $p = -\rho$ corresponds to the de Sitter vacuum and generates, via the Einstein equations, $G_{\mu\nu} = -(8\pi G/c^2)T_{\mu\nu}$, the de Sitter geometry, described by line element (2) with the metric function

$$g(r) = 1 - \frac{r^2}{r_\Lambda^2}; \quad r_\Lambda^2 = \frac{3c^2}{8\pi G\rho_\Lambda}; \quad \rho_\Lambda = (8\pi G/c^2)^{-1}\Lambda \tag{3}$$

where r_Λ is the de Sitter curvature radius, ρ_Λ is the vacuum density related to the cosmological constant Λ which is, constant by virtue of the contracted Bianchi identities $G^\mu_{\nu;\mu} = 0$, and $\mu, \nu = 0, 1, 2, 3$.

The de Sitter geometry is characterized by the constant positive non-zero curvature $R = 4\Lambda$. In the observer region spacetime is described by the Minkowski geometry with zero curvature $R = 0$. Spontaneous symmetry breaking of scalar fields from the false to the true vacuum state involves thus breaking of spacetime symmetry from the de Sitter group to the Poincaré group [1].

The de Sitter gravity induced in the interaction vertex implies that it should have to be gravito-electroweak. The de Sitter spacetime symmetry requires description of a particle mass square by the eigenvalue of the Casimir operator I_1 in the de Sitter space, defined as [35]

$$I_1 = -\Pi_\mu \Pi^\mu - \frac{1}{2r_\Lambda^2} J_{\mu\nu} J^{\mu\nu}; \quad \Pi_\mu = \left(1 + \frac{r^2 - c^2 t^2}{4r_\Lambda^2} \right) P_\mu + \frac{1}{2r_\Lambda^2} x^\nu J_{\mu\nu} \tag{4}$$

where $J_{ij} = -J_{ji} = \epsilon_{ijk} J_k$, $J_{i0} = -J_{0i} = -K_i$; $i, j, k = 1, 2, 3$. The operator I_1 can be written as

$$I_1 = P_\mu P^\mu \left(1 + \frac{r^2 - c^2 t^2}{4r_\Lambda^2} \right)^2 - \frac{1}{r_\Lambda^2} (\mathbf{J}^2 - \mathbf{K}^2). \tag{5}$$

The operators \mathbf{J} and \mathbf{K} are generators of rotations and of the Lorentz boosts given by [36]

$$\mathbf{J}_R = \hbar \frac{\boldsymbol{\sigma}}{2}, \quad \mathbf{K}_R = -i\hbar \frac{\boldsymbol{\sigma}}{2}; \quad \mathbf{J}_L = \hbar \frac{\boldsymbol{\sigma}}{2}, \quad \mathbf{K}_L = +i\hbar \frac{\boldsymbol{\sigma}}{2}. \tag{6}$$

The indices R and L mark the right-handed and left-handed fields; $\boldsymbol{\sigma}$ denotes the Pauli matrices (the Pauli vector).

The Casimir operator I_1 and its eigenvalue I'_1 take the form [13]

$$I_1 = P_\mu P^\mu \left(1 + \frac{r^2 - c^2 t^2}{4r_\Lambda^2} \right)^2 - \frac{\hbar^2}{2r_\Lambda^2} \sigma^2; I'_1 = m^2 c^2 \left(1 + \frac{r^2 - c^2 t^2}{4r_\Lambda^2} \right)^2 - \frac{3\hbar^2}{2r_\Lambda^2}. \tag{7}$$

In the limit $r_\Lambda \rightarrow \infty$ corresponding to the Minkowski geometry, I'_1 reduces to the Poincaré invariant $P_\mu P^\mu = m^2 c^2$. The de Sitter invariant I'_1 involves the Poincaré mass square and the angular momentum of a particle [35]. The de Sitter eigenvalue is modified as compared with the Poincaré eigenvalue. The modification includes the dependence on the curvature radius and appearance of an additional negative term originated from the intrinsic involvement of the de Sitter geometry, which can (but must not) dominate and then lead to the appearance of the negative mass squares [12,13]. The first term in (7) depends on the curvature radius r_Λ and essentially involves a neutrino (Poincaré) mass, still unknown. Therefore, we can choose the second term, which depends only on the geometry, as the scale parameter characterizing the involvement of gravity and spacetime symmetry

$$m_{neg}^2 = \frac{3\hbar^2}{2r_\Lambda^2}. \tag{8}$$

to get some qualitative estimate for a gravito-electroweak scale at least by the order of magnitude.

The de Sitter curvature radius r_Λ depends on the density of the de Sitter vacuum ρ_Λ as $r_\Lambda^2 = 3c^2 / (8\pi G \rho_\Lambda)$, and provides the dependence of the mass square in (8) on the de Sitter vacuum density ρ_Λ [13]

$$m_{neg}^2 = \frac{4\pi\hbar^2 G}{c^4} \rho_\Lambda. \tag{9}$$

To connect ρ_Λ with a gravito-electroweak mass scale M_{GeW} as compared with the Planck scale, we express the relation between ρ_Λ and M_{GeW} in the way corresponding to the relation between ρ_{Pl} and M_{Pl} , which is $\rho_{Pl} = M_{Pl} / (l_{Pl})^3$, where $l_{Pl} = \hbar / (M_{Pl} c) = \sqrt{\hbar G / c^3}$ and $M_{Pl} = \sqrt{\hbar c / G}$. Applying $\rho_\Lambda = M_{GeW} / (\hbar / M_{GeW} c)^3$ we obtain $\rho_\Lambda = (c^3 / \hbar^3) M_{GeW}^4$ and find from Equation (9) the relation between m_{neg}^2 and M_{GeW}

$$m_{neg}^2 = 4\pi \left(\frac{M_{GeW}}{M_{Pl}} \right)^4 M_{Pl}^2 \tag{10}$$

The scale M_{GeW} is expressed through m_{neg}^2 as

$$M_{GeW} = \left(\frac{m_{neg}^2}{4\pi M_{Pl}^2} \right)^{1/4} M_{Pl}. \tag{11}$$

This formula relates the value of M_{GeW} with the scale for the negative mass square value, currently accessible from experiments. Choosing for the scale parameter the value $m_{neg}^2 \simeq 1 \text{ eV}^2$ from the recently reported value $m_v^2 = (-1.0^{+0.9}_{-1.1}) \text{ eV}^2$ [31] and taking into account that $M_{Pl} = 1.22 \times 10^{19} \text{ GeV}$, we get an estimate $M_{GeW} \simeq 58.7 \text{ TeV}$, consistent with predictions of theories of the gravito-electroweak unification [37–39].

3. Minimal Length In $e^+e^- \rightarrow \gamma\gamma(\gamma)$ Annihilation

The data on the annihilation reaction $e^+e^- \rightarrow \gamma\gamma(\gamma)$ from VENUS, TOPAZ, ALEPH, DELPHI, L3, OPAL collaborations have been collected and worked out for about fifteen years at the energies from $\sqrt{s} = 55 \text{ GeV}$ to 207 GeV [14,15]. The χ^2 fit, shown in Figure 1, displays with the 5σ significance at a minimum with a negative QED fit parameter $(1/\Lambda^4)_{best} \simeq -1.1 \times 10^{-10} \text{ GeV}^{-4}$ where Λ is the

QED cutoff parameter, corresponding to the maximal resolution $l_e \simeq 1.57 \times 10^{-17}$ cm at the energy $E = 1.253$ TeV [14,15].

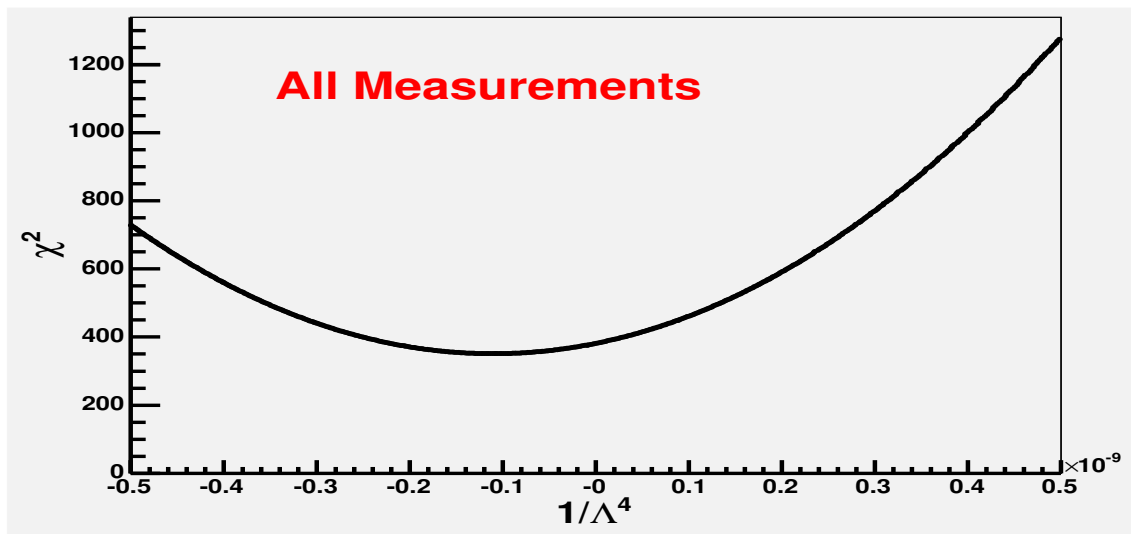


Figure 1. A minimum in the χ^2 fit with $P = 1/\Lambda^4$.

The χ^2 test was performed with the QED hypotheses which predicted an increase in the total QED- α^3 cross section. Instead, we see in Figure 1 the minimum with the negative value of the QED fit parameter. The applied standard QED techniques assume a point-like conception of a particle. Cross section would be modified in the case when characteristic test distances are smaller than a particle size. The Compton wavelength of the electron $\lambda_e = \hbar/(m_e c) = 3.9 \times 10^{-11}$ cm and its classical radius $r_e = e^2/(m_e c^2) = 2.8 \times 10^{-13}$ cm substantially exceed the test length $l_e = 1.57 \times 10^{-17}$ cm, and description of annihilating particles requires an approach of an extended particle.

The early studies on an extended electron models revealed the need in introducing cohesive forces of non-electromagnetic origin [40] required to balance the Coulomb repulsion (for a review, see [15]). In the Nonlinear Electrodynamics coupled to Gravity this role is played by the repulsive gravity of the de Sitter vacuum. The regular NED-GR solutions describe in the self-consistent way, without additional assumptions except the Weak Energy Condition (WEC), electrically charged spinning solitons with the de Sitter vacuum interiors. Their electromagnetic fields are described by the source-free dynamical field equations. The gravitational field is generated by stress-energy tensors for the nonlinear electromagnetic fields which are defined by ([41] and references therein)

$$T^{\mu}_{\nu} = -2\mathcal{L}_F F_{\nu\alpha} F^{\mu\alpha} + \frac{1}{2}\delta^{\mu}_{\nu} \mathcal{L}; \quad \mathcal{L}_F = d\mathcal{L}/dF \tag{12}$$

and generically satisfies the condition (1) which ensures the existence of the de Sitter interiors. The regular axially symmetric metrics are obtained from the regular spherical metrics (2) by the Gürses-Gürsey formalism [42] which includes the Newman-Janis complex coordinates transformation [43] typically applied for obtaining the axial metrics.

In the Boyer-Lindquist coordinates, the metric is given by [42]

$$ds^2 = \frac{2f - \Sigma}{\Sigma} dt^2 + \frac{\Sigma}{\Delta} dr^2 + \Sigma d\theta^2 - \frac{4af \sin^2 \theta}{\Sigma} dt d\phi + \left(r^2 + a^2 + \frac{2fa^2 \sin^2 \theta}{\Sigma} \right) \sin^2 \theta d\phi^2 \tag{13}$$

where

$$\Sigma = r^2 + a^2 \cos^2 \theta; \quad \Delta = r^2 + a^2 - 2f(r); \quad f(r) = r\mathcal{M}(r) \tag{14}$$

and the Lorentz signature is $[- + + +]$. For spherical solutions satisfying WEC, an object has the positive mass, and the mass function $\mathcal{M}(r)$ evolves monotonically from $\mathcal{M}(r) = 4\pi\rho(0)r^3/3$ as $r \rightarrow 0$ to $\mathcal{M}(r) = m - e^2/2r$ as $r \rightarrow \infty$ [41], where m is the gravitational mass, and the metric (2) goes to the Kerr–Newman vacuum metric with the associated electromagnetic potential $A_i = -(er/\Sigma)[1; 0, 0, -a \sin^2 \theta]$, published in 1965 [44].

Comprehensive analysis of the Kerr–Newman solution by Carter in 1968 revealed its remarkable possibility to present the electron as seen by a distant observer, because the angular momentum $J = ma$ and the asymptotic magnetic momentum $\mu = ea$ result in the gyromagnetic ratio $g = 2$ corresponding to a spinning particle [45]. The charge e as a constant of integration of dynamical equations for electromagnetic fields.

Carter discovered the nontrivial causality violation in the Kerr–Newman spacetime due to existence in the interior region of closed time-like curves which can be extended over the whole manifold [45]. Since then, the electron models have been constructed by matching the Kerr–Newman solution for the exterior fields with some interior material source (for a review, see [15,46]). Contemporary models include the models with the superconducting interior with the Minkowski geometry confined by the domain wall boundary ([47,48] and references therein), and the models dominated by dynamical role of the electron spin ([49–51] and references therein).

The problem of matching the Kerr–Newman vacuum solution to a material interior source does not have a unique solution, due to arbitrariness in the boundary between the exterior and interior [52]. In NED-GR, this problem does not arise. An electromagnetic spinning solution is made of a nonlinear electromagnetic field and bound by the gravitational interaction. Its basic generic properties can be found by the analysis of asymptotic behavior of regular solutions.

In geometry (13), the surfaces $r = \text{constant}$ are the confocal ellipsoids

$$r^4 - (x^2 + y^2 + z^2 - a^2)r^2 - a^2z^2 = 0 \tag{15}$$

degenerated to the equatorial disk $r = 0$ defined by

$$x^2 + y^2 \leq a^2, \quad z = 0 \tag{16}$$

and confined by the ring $x^2 + y^2 = a^2, \quad z = 0$ [53].

The function $f(r)$ in (13) and (14) provides the direct connection of the axial solution with the density profile $\tilde{\rho}(r)$ of an original spherical solution. The prime denotes the derivative with respect to r . The eigenvalues of a stress–energy tensor (12) in the co-rotating references frame with the angular velocity $\omega(r) = u^\phi/u^t = a/(r^2 + a^2)$, are given by $\Sigma^2\rho = 2(f'r - f)$; $p_r = -\rho$; $\Sigma^2p_\perp = 2(f'r - f) - f''\Sigma$ [42], where p_\perp is the transversal pressure.

In the equatorial plane $(p_\perp + \rho) = -r^3\tilde{\rho}'(r)/2\Sigma$ [16]. For the spherical solutions satisfying WEC regularity requires $r\tilde{\rho}'(r) \rightarrow 0$ as $r \rightarrow 0$ [41]. As a result on the disk (16), $p_\perp + \rho = 0 \rightarrow p_\perp = p_r = p$, and the equation of state

$$p = -\rho \tag{17}$$

represents the rotating de Sitter vacuum in the co-rotating frame [16].

In geometry, with the metric (13) the non-zero field components $F_{01}, F_{02}, F_{13}, F_{23}$ are connected by

$$F_{31} = a \sin^2 \theta F_{10}; \quad aF_{23} = (r^2 + a^2)F_{02} \tag{18}$$

so that the electromagnetic field is presented by two independent field functions. The field invariant $F = F_{ik}F^{ik}$ reads

$$F = 2 \left(\frac{F_{20}^2}{a^2 \sin^2 \theta} - F_{10}^2 \right). \tag{19}$$

The density and pressure are created by the electromagnetic fields and given by [16]

$$\rho = \frac{1}{2}\mathcal{L} + 2\mathcal{L}_F F_{10}^2; \quad p_r = -\rho; \quad p_\perp = -\frac{1}{2}\mathcal{L} + 2\mathcal{L}_F \frac{F_{20}^2}{a^2 \sin^2 \theta}. \tag{20}$$

This leads to

$$p_\perp + \rho = 2\mathcal{L}_F \left(F_{10}^2 + \frac{F_{20}^2}{a^2 \sin^2 \theta} \right). \tag{21}$$

Presented in the literature are regular spherical solutions with the non-zero electric charge [41,54–57], which have been obtained in the alternative *P*-frame of nonlinear electrodynamics connected with the standard Lagrangian *F*-form by the Legendre transformation [58]. The *F*-*P* duality coincides with the usual electric–magnetic duality only in the Maxwell weak field limit. In general, the Legendre transformation connects the different theories [59].

In the spherically symmetric case integration of the electromagnetic field equation yields $F = -2e^2 / \mathcal{L}_F^2 r^4$ [41,59], which leads to $F\mathcal{L}_F^2 \rightarrow -\infty$ as $r \rightarrow 0$. The form of a stress–energy tensor implies $p_\perp + \rho = F\mathcal{L}_F$, regular solutions have obligatory de Sitter center, where $p_\perp + \rho = 0$ and hence $F\mathcal{L}_F = 0$. Regularity requires thus $\mathcal{L}_F \rightarrow \infty$ and $F \rightarrow -0$ when $r \rightarrow 0$ [41,59]. In the Maxwell region $F \rightarrow -0$ as $r \rightarrow \infty$. Non-monotonic behavior of the invariant *F* results in branching of a Lagrangian $\mathcal{L}(F)$ in the extremum *F*. Branching of a Lagrangian requires the description of the Lagrange dynamics by the non-uniform variational problem with the action [60]

$$\mathcal{I} = \mathcal{I}_{int} + \mathcal{I}_{ext} = \frac{1}{16\pi} \left[\int_{\Omega_{int}} (R - \mathcal{L}_{int}(F)) \sqrt{-g} d^4x + \int_{\Omega_{ext}} (R - \mathcal{L}_{ext}(F)) \sqrt{-g} d^4x \right]. \tag{22}$$

The regions Ω_{int} and Ω_{ext} are bounded by the space-like hypersurfaces $t = t_{in}$ and $t = t_{fin}$. The region Ω_{ext} is bounded at infinity by the time-like three-surface at which the electromagnetic fields zero out in the Maxwell limit. Internal boundary between Ω_{int} and Ω_{ext} is presented by a time-like hypersurface Σ_c at the extremum of the field invariant *F* [60].

In the case of the minimal coupling variation in the action (22) results, in both Ω_{int} and Ω_{ext} , in the dynamical equations for the electromagnetic field

$$\nabla_\mu (\mathcal{L}_F F^{\mu\nu}) = 0; \tag{23}$$

$$\nabla_\mu {}^*F^{\mu\nu} = 0; \quad {}^*F^{\mu\nu} = \frac{1}{2} \eta^{\mu\nu\alpha\beta} F_{\alpha\beta}; \quad \eta^{0123} = -\frac{1}{\sqrt{-g}}, \tag{24}$$

and the Einstein equations $G_{\mu\nu} = -8\pi G T_{\mu\nu}$ with the stress–energy tensor of an electromagnetic field (12). The standard boundary conditions on the surface Σ_c read [60]

$$\int_{\Sigma_c} \left(\mathcal{L}_{F(int)} F_{\mu\nu(int)} - \mathcal{L}_{F(ext)} F_{\mu\nu(ext)} \right) \sqrt{-g} \delta A^\mu d\sigma^\nu = 0; \quad \mathcal{L}_{int} - 2\mathcal{L}_{F(int)} F_{int} = \mathcal{L}_{ext} - 2\mathcal{L}_{F(ext)} F_{ext} \tag{25}$$

The dynamic Equations (23) and (24) form the system of four equations.

In the axially symmetric case, the regular solutions to the dynamical Equation (23) are given by [16,17]

$$\Sigma^2 (\mathcal{L}_F F_{01}) = -e(r^2 - a^2 \cos^2 \theta); \quad \Sigma^2 (\mathcal{L}_F F_{02}) = ea^2 r \sin 2\theta; \tag{26}$$

$$\Sigma^2 (\mathcal{L}_F F_{31}) = ae \sin^2 \theta (r^2 - a^2 \cos^2 \theta); \quad \Sigma^2 (\mathcal{L}_F F_{23}) = aer (r^2 + a^2) \sin 2\theta. \tag{27}$$

In the Maxwell limit $\mathcal{L}_F = 1$, these functions are solutions to the system (23) and (24) and coincide with the solutions obtained in the Kerr–Newman geometry [45,61].

The field components (26) and (27) satisfy two equations (23) and the condition of compatibility of the system of four Equations (23) and (24) for two independent functions F_{20}, F_{10} [17]. Detailed analysis shows that, in addition to the Maxwell weak field limit, the functions (26) and (27) satisfy the total

dynamical system (23) and (24) as the regular asymptotic solutions in the strongly nonlinear regime $\mathcal{L}_F \rightarrow \infty$ on the disk where the electromagnetic density achieves the maximal value [17,46].

Applying solutions (26) and (27) on the disk (16) we get relations [16,17]

$$\mathcal{L}_F = \frac{2e^2}{\Sigma^2(p_\perp + \rho)}; F = -\frac{(p_\perp + \rho)^2 \Sigma^2}{2e^2}. \tag{28}$$

It follows that $F \rightarrow -0$ approaching the disk, while $\mathcal{L}_F \rightarrow \infty$.

In terms of the field intensities defined by [16,62]

$$E_j = \{F_{j0}\}; D^j = \{\mathcal{L}_F F^{0j}\}; B^j = \{^*F^{j0}\}; H_j = \{\mathcal{L}_F ^*F_{0j}\}; j = 1, 2, 3 \tag{29}$$

the dynamical Equations (23) and (24) take the standard form of the source-free Maxwell equations

$$\nabla \cdot \mathbf{D} = 0; \nabla \times \mathbf{H} = \frac{\partial \mathbf{D}}{\partial t}; \nabla \cdot \mathbf{B} = 0; \nabla \times \mathbf{E} = -\frac{\partial \mathbf{B}}{\partial t}. \tag{30}$$

The electric induction \mathbf{D} and the magnetic induction \mathbf{B} are related with the electric and magnetic field intensities by

$$D^j = \epsilon_k^j E^k; B^j = \mu_k^j H^k, \tag{31}$$

where ϵ_j^k and μ_j^k are the tensors of the electric and magnetic permeability given by [16]

$$\epsilon_r^r = \frac{(r^2 + a^2)}{\Delta} \mathcal{L}_F; \epsilon_\theta^\theta = \mathcal{L}_F; \mu_r^r = \frac{(r^2 + a^2)}{\Delta \mathcal{L}_F}; \mu_\theta^\theta = \frac{1}{\mathcal{L}_F}. \tag{32}$$

In accordance with the basic relations (28) $\mathcal{L}_F \rightarrow \infty$ at the disk, and hence the magnetic permeability $\mu_r^r = \mu_\theta^\theta = 1/\mathcal{L}_F$ goes to zero, while the electric permeability $\epsilon_r^r = \epsilon_\theta^\theta = \mathcal{L}_F$ goes to infinity. The disk (16) displays the properties of a perfect conductor and ideal diamagnetic [16,17].

The surface current on the disk is defined by $4\pi j_k = [e_{(k)}^\alpha F_{\alpha\beta} n^\beta]$, where $e_{(k)}^\alpha$ are the base vectors related to the intrinsic coordinates $t, \phi, 0 \leq \xi \leq \pi/2$, the vector $n_\alpha = \delta_\alpha^1 (1 + q^2/a^2)^{-1/2} \cos \xi$ is the unit normal to the disk, and the symbol [..] denotes a jump in the orthogonal direction [52]. On the de Sitter disk, where $\mu_r^r = \mu_\theta^\theta = \mu$, this gives [63]

$$j_\phi = -\frac{ec}{2\pi a} \sqrt{1 + e^2/a^2} \sin^2 \xi \frac{\mu}{\cos^3 \xi}. \tag{33}$$

The current j_ϕ vanishes over the disk surface, due to $\mu = 0$, but on the confining ring $\xi = \pi/2$, both terms in the second fraction go to zero independently, so that the current can be any amount to a non-zero total value, which is the basic general criterion for a superconducting current [64]. Since this current flows without resistance in the perfect conductor region, it represents a non-dissipative source of the electromagnetic fields, which can provide an unlimited lifetime of an object [63].

In the case of the electron $mac = \hbar/2$, the superconducting current which produces its electromagnetic fields, as well as geometry (13), can be calculated through its known magnetic momentum μ_{in} , which is intrinsic because the dynamical Equations (23) and (24) are source-free [65]. Approaching the disk, $2f(r) \rightarrow r^4/r_\Lambda^2 \rightarrow 0$ ($r_\Lambda^2 = 3/8\pi G\rho(0)$), so the disk is intrinsically flat [16] and $\mu_{in} = c^{-1} j_\phi S$ where S is the disk area. Introducing the uncertain coefficient in (33), $j_\phi = -(ec/2\pi a) \sqrt{1 + e^2/a^2} U$, so we restore it from the formula for the magnetic momentum, $\mu_{in} = -(eS/2\pi a) \sqrt{1 + q^2/a^2} U$, and obtain the superconducting current which powers the electron at the value $j_\phi = 79.277 \text{ A}$ [65].

In the region of a distant observer $r \gg \lambda_e$ it generates the electric and magnetic fields [63]

$$E_r = -\frac{e}{r^2} \left(1 - \frac{\hbar^2}{m_e^2 c^2} \frac{3 \cos^2 \theta}{4r^2} \right); E_\theta = \frac{e\hbar^2}{m_e^2 c^2} \frac{\sin 2\theta}{4r^3}; \tag{34}$$

$$B^r = -\frac{e\hbar}{m_e c} \frac{\cos \theta}{r^3} = 2\mu_e \frac{\cos \theta}{r^3}; B_\theta = -\mu_e \frac{\sin \theta}{r^4}. \tag{35}$$

In terms of the Coleman lump, the leading term in E_r yields the Coulomb law in the classical limit $\hbar = 0$, while the higher terms represent the quantum corrections [63].

For the purely electromagnetic interaction $e^+e^- \rightarrow \gamma\gamma(\gamma)$, the case of the minimal length in annihilation can be approached by generic properties of spinning electromagnetic soliton, which offer a physical mechanism responsible for appearance of the minimal length due to involving gravity and the de Sitter vacuum able to prevent a formation of singularities by its intrinsic negative pressure. The gravitational acceleration, $\ddot{a} \propto -a(\rho + 3p)$ in the de Sitter vacuum with $p = -\rho$ is repulsive.

Regular NED-GR solutions provide the de Sitter cutoff on self-interaction. Comparing electromagnetic self-energy density with the energy density of the de Sitter vacuum [41]

$$\frac{e^2}{r_c^4} \simeq 8\pi G\rho_\Lambda = \frac{3}{r_\Lambda^2} \tag{36}$$

in which we obtain $r_c \simeq 1.05 \times 10^{-17}$ cm as a rough qualitative estimate, which appears close to l_e [15].

For more detailed analysis, we take into account that, at a certain stage of the annihilation process, the interaction region becomes neutral and spinless and can be considered as a spherical bubble with the de Sitter interior and the Schwarzschild exterior. The metric of this bubble is described by (2), and the typical behavior of a metric function is shown in Figure 2 (left) [20]. The mass parameter is normalized to the critical value, corresponding to the double horizon. The curve with $m > 1$ represents a regular black hole, and the case $m < 1$ corresponds to a spherical bubble without horizons.

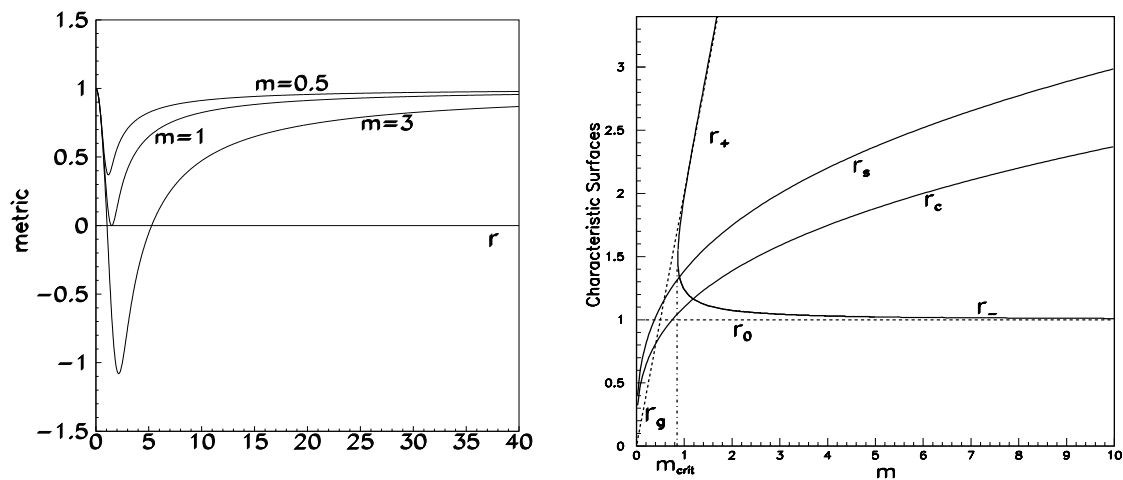


Figure 2. (Left) Typical behavior of a metric function $g(r)$ for a spherical lump. (Right) Radius r_c of the surface of zero gravity and r_s of the surface of zero curvature.

In geometry, with the de Sitter center, there exists the surface of the zero gravity surface $r_c \sim (r_\Lambda^2 r_g)^{1/3}$ where the r_Λ is the de Sitter radius and $r_g = 2Gm$ is the surface $r = r_s$ the curvature scalar $R = 8\pi GT$ changes its sign.

Adopting for the de Sitter vacuum, the electroweak scale $E_{EW} = 246$ GeV responsible for the electron mass [66], we obtain the value of the de Sitter radius $r_\Lambda = 1.374$ cm. For a lump with the energy $E \simeq 1.253$ TeV, the radius of zero gravity surface is $r_c \sim 0.86 \times 10^{-16}$ cm, so that the length $l_e = 1.57 \times 10^{-17}$ cm fits within the region with the repulsive gravity.

The minimal length l_e can be understood as a characteristic distance at which the electromagnetic attraction is balanced by the gravitational repulsion of the de Sitter vacuum [15].

4. DM Candidates with the de Sitter Vacuum Interiors

Here we outline the more realistic (for our Universe) case of regular black hole remnants and G-lumps in the space with non-zero cosmological constant, and their observational signatures related to the Higgs mechanism and de Sitter spacetime symmetry.

Analysis of spherically symmetric Einstein equations has shown that regular solutions of the Kerr–Schild class, specified by (1) and described by the metrics (2), have obligatory de Sitter centers [7,67]. Repulsive gravity of the de Sitter vacuum prevents the formation of a singularity in accordance with the early hypothesis of a geometry self-regulation [68], of the existence of the limiting value of spacetime curvature [69], of spacetime symmetry restoration on the GUT scale [20,70,71]—confirmed later in the frame of quadratic gravity [72]—of renormalization group improvement [73], of non-commutative geometry approach [74], and of an ultraviolet quantum gravity [75,76] (for a recent review, see [25,77]).

Spacetime with the de Sitter center in the universe with the non-zero cosmological constant λ has not more than three horizons [78]. The metric function $g(r)$ in (2) has the form [79]

$$g(r) = 1 - \frac{2G\mathcal{M}(r)}{r} - \frac{\lambda}{3}r^2; \quad \mathcal{M}(r) = 4\pi \int_0^r \rho(x)x^2 dx \tag{37}$$

where the density $\rho(r)$ tends to the de Sitter density ρ_Λ as $r \rightarrow 0$. A stress–energy tensor responsible for this metric evolves from $T_k^i = (\rho_\Lambda + \rho_\lambda)\delta_k^i$ at the center to $T_k^i = \rho_\lambda\delta_k^i$ at infinity.

The evolution between two de Sitter vacua is ensured by the algebraic structure of a stress–energy tensor for this class of solutions, which is specified by (1), represents a particular case of a vacuum with the reduced symmetry [22,70] (vacuum equation of state only in one or two spatial direction(s), $p_\alpha = -\rho$), and can be identified as an anisotropic quintessence ([80] and references therein). Quintessence was originally introduced as an isotropic medium by the equation of state $p = w\rho$ with $-1 < w < 0$ [81]. In the anisotropic case, the definition extends to $p_\alpha = w_\alpha\rho$, $w_\alpha = -1$ and $p_\beta = w_\beta\rho$, $\beta \neq \alpha$, where $w_\beta \geq -1$. In general, it is coordinate-dependent and represents a time-evolving and spatially inhomogeneous dark energy, which can provide evolution between de Sitter vacua with the different values of the cosmological constant [80].

In the here-considered case, a medium specified by $T_t^t = T_r^r$ satisfies the r –dependent equation of state [70]

$$p_r = -\rho; \quad p_\perp = -\rho - r\rho'/2 \tag{38}$$

and is identified as an anisotropic quintessence defined by two EOS parameters, w_r and w_\perp , related to principal pressures as $p_r = w_r\rho$, $w_r = -1$; $p_\perp = w_\perp\rho$, $w_\perp = -1 - (r/2)d(\ln\rho)/dr$ [23]. In our case, T_t^t satisfies WEC, which requires $p_\perp + \rho \geq 0$ and leads to $\rho' \leq 0$. As a result, the density increases towards the center, where the spacetime symmetry restores to the de Sitter group [7,67] (see also [77] and references therein).

Geometry has three basic length scales $r_g, r_\Lambda, r_\lambda$ and is characterized also by the parameter q relating de Sitter vacuum scales

$$r_g = 2GM; \quad r_\Lambda = \sqrt{3/\Lambda}; \quad r_\lambda = \sqrt{3/\lambda}; \quad q = r_\lambda/r_\Lambda = \sqrt{\Lambda/\lambda} = \sqrt{\rho_\Lambda/\rho_\lambda}; \quad \rho_{\Lambda(\lambda)} = (8\pi G)^{-1}\Lambda(\lambda) \tag{39}$$

where $M = 4\pi \int_0^\infty \rho(r)r^2 dr$ is the mass.

The metric function tends for $r \rightarrow 0$ to the de Sitter metric with $g(r) = 1 - r^2(\Lambda + \lambda)/3$, for $r_g/r \rightarrow 0$ to the Schwarzschild–de Sitter metric function $g(r)_{Schw-deS} = 1 - 2GM/r - \lambda r^2/3$, and for $r \rightarrow \infty$ tends to the de Sitter metric function $g(r) = 1 - \lambda r^2/3$.

The relevant spacetime configurations are shown in Figure 3.

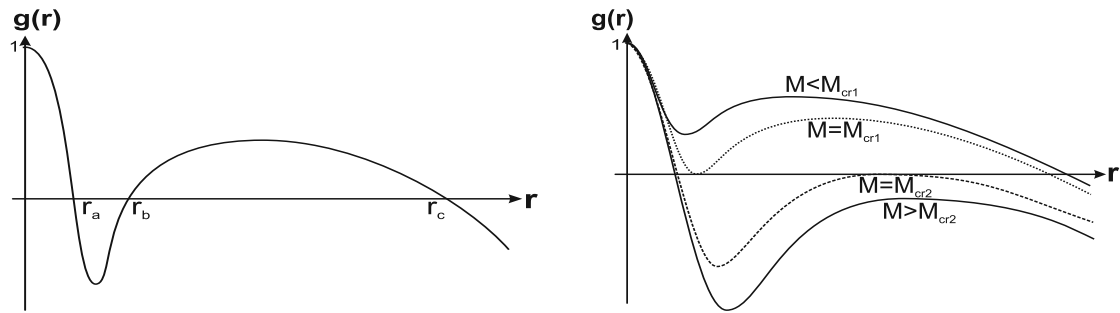


Figure 3. Typical behavior of the metric function $g(r)$ for the case of two vacuum scales.

They include a regular cosmological black hole with the mass within the range $M_{cr1} < M < M_{cr2}$, bounded by the event horizon r_b and the internal horizon r_a in the universe with the cosmological horizon r_c (Figure 3, left); two double-horizon states, $r_a = r_b$ ($M = M_{cr1}$) and $r_b = r_c$ ($M = M_{cr2}$), and two one-horizon states (Figure 3, right). The case $M < M_{cr1}$ (Figure 1, right) presents G-lumps replacing naked singularities.

Mass of all objects is generically related to interior de Sitter vacuum and breaking of spacetime symmetry from the de Sitter group [7].

The quantum temperature and the entropy of a horizon [82], and its specific heat [83] are given by:

$$kT_h = \frac{\hbar c}{4\pi} |g'(r_h)|; S_h = 4\pi r_h^2; C_h = dE_h/dT_h = \frac{2\pi r_h}{g'(r_h) + g''(r_h)r_h}. \tag{40}$$

Typical behavior of the temperature and the specific heat capacity during evaporation is shown in Figure 4. As follows from (40), temperature vanishes on the double horizons, hence it must have a maximum somewhere in between. In the maximum, a specific is broken and changes sign, testifying for a 2nd order phase transition in the course of quantum evaporation [20,83,84].

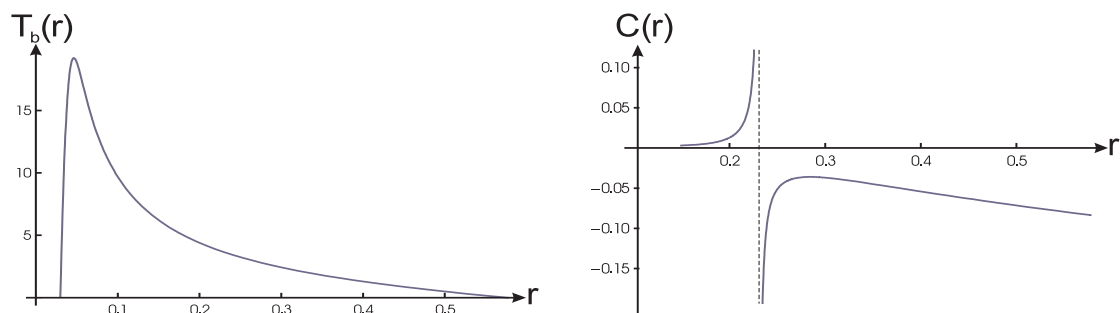


Figure 4. Generic behavior of temperature (left) and of specific heat (right) of the black hole event horizon.

The internal black hole horizon is the cosmological horizon for an observer in the region $0 \leq r < r_a$. It moves outwards in accordance with the 2nd Law of thermodynamics as well as the cosmological horizon r_c . Behavior of the total mass M is determined by the behavior of $g'(r)$ and is directed to its decreasing during evaporation. As a result, the black hole event horizon shrinks. This behavior imposes a certain constraint on the density profile, which has to involve scaling r/r_* [83,85] (for a review, see [24,86]). The black hole evaporation stops at the double-horizon state, $r_a \rightleftharpoons r_b$ (the curve $M = M_{cr1}$ in Figure 1, right), where the temperature zeroes out at the positive specific heat in accordance with (40). A regular black hole leaves behind a thermodynamically stable double-horizon remnant with the de Sitter vacuum interior. Its mass is given by $M_{remn} = M_{cr1} = \beta M_{Pl} \sqrt{\rho_{Pl}/\rho_\Lambda}$ [20,83], where the numerical coefficient β depends on the particular form of the density profile $\rho(r)$.

The density profile applied for plotting the pictures illustrating generic behavior, describes the semiclassical model of the vacuum polarization in the spherical gravitational field [70]

$$\rho(r) = \rho_{\Lambda} e^{-r^3/r_*^3}; \quad \mathcal{M}(r) = M(1 - e^{-r^3/r_*^3}) \quad (41)$$

in the frame of the hypothesis of symmetry restoration in a gravitational collapse due to the fact that all fields are involved in a collapse and contribute to vacuum polarization [7,20,70]. In this geometry the scale r_* determines the radius of the surface of zero gravity by $r_c = (2/3)^{1/3}r_*$ and the radius of the surface of zero curvature by $r_s = (4/3)^{1/3}r_*$ [20,70].

Observational Signatures of Remnants and G-lumps

Black hole remnants have been considered as a reliable source of dark matter for more than three decades [87,88] (for a recent review, see Reference [89]). Regular black hole remnants are free of the existential problem encountered by singular remnants because of the absence of a reliable mechanism preventing complete evaporation [90,91]. Regular remnants and G-lumps are stable DM candidates with the de Sitter vacuum interiors, which can be confirmed by their observational signatures. Their stability to external perturbations are regulated by the general criteria applicable for a wide class of the density profiles [92,93].

Regular primordial black holes, their remnants and G-lumps with the interior de Sitter vacuum can arise in a quantum collapse of primordial fluctuations during the phase transition in the early Universe, including the first and second (100–200 MeV [94]) inflationary stages, supported by the de Sitter vacuum. They can capture available charged particles and form graviatoms—gravitationally bound, $\alpha_G = GMm/\hbar c$, quantum systems [95].

The mass of regular remnants with the de Sitter vacuum at the GUT scale is estimated as 10^2 – 10^3 g [20]. Therefore, remnants, G-lumps and graviatoms are classified as heavy DM candidates with DE interiors (for a review, see [25]).

Information on the interior de Sitter vacuum can be presented by the observational signature for graviatoms. The characteristic frequency of their electromagnetic radiation depends on the scale of the de Sitter vacuum E_{int} [95]. For the density profile (41) the energy $\hbar\omega = 0.678 \hbar c/r_{\Lambda} = 0.678 \times 10^{11} \text{ GeV} (E_{int}/E_{GUT})^2$ fits within the range available for observations possibilities (cosmic photons are detected for energy up to $10^{11.5}$ GeV [96]).

The most promising observational signature of the regular remnants, G-lumps and graviatoms with the GUT scale interiors is directly related to the de Sitter vacuum $p = -\rho$ which is the false vacuum of the Higgs mechanism. In the GUT false vacuum interiors of regular remnants and G-lumps, non-conservation of the baryon and lepton numbers may lead to the gravitational capture of the proton in an underground detector, followed by induced proton decay [26]. For the cross-section of induced proton decay $\sigma_i \sim 10^{-26} \text{ cm}^2$, one can expect about one event per 10^7 years in one ton of an underground detector. In the matter of a 1 km^3 detector, such as IceCUBE, there should be up to 300 events per year. In the graviatom, its remnant component can induce nucleon decay, while the charged component provides the enhancement of the cross section [26].

This observational signature makes heavy DM search at the IceCUBE experiment challenging, also in connection with the predicted in supergravity unified model's [27] sensitivity of the proton lifetime to the Higgs boson mass. A small (few GeV) shift in its mass can change the proton decay lifetime up to two orders of magnitude [27].

5. Conclusions

The basic essential feature of the Higgs mechanism is spontaneous symmetry breaking of scalar fields from a false vacuum state $p = -\rho$ to the true vacuum state $p = \rho = 0$. The false vacuum equation of state $p = -\rho$ corresponds to the maximally symmetric de Sitter vacuum with the nonzero constant vacuum density related to the cosmological constant, $\Lambda = 8\pi G\rho_{\Lambda}$. The de Sitter vacuum

generates, by the Einstein equations, the de Sitter geometry with nonzero positive constant curvature $R = 4\Lambda$. Hence the Higgs mechanism intrinsically incorporates the de Sitter spacetime symmetry in the region of interaction and breaking of spacetime symmetry from the de Sitter group to the Poincaré group, which corresponds to the Minkowski geometry with zero curvature, $R = 0$. Spontaneous symmetry breaking of scalar fields involves thus the relevant breaking of the spacetime symmetry.

The generic relation of the Higgs mechanism with the spacetime symmetry and with the de Sitter gravity is displayed in the currently reported data on negative mass squares for neutrinos and in the appearance of the minimal length in the electron–positron annihilation $e^+e^- \rightarrow \gamma\gamma(\gamma)$.

The de Sitter spacetime symmetry in the interaction vertex makes it gravito-electroweak and requires application of the Casimir operators in the de Sitter geometry for description of a particle state. The first Casimir invariant responsible for a particle mass, $P_\mu P^\mu = m^2 c^2$ in the Minkowski geometry, involves the dependence on the de Sitter curvature radius $r_\Lambda = \sqrt{3/(8\pi G\rho_\Lambda)}$, including the additional negative term which depends only on geometry. In the case of neutrinos, this term can dominate due to extreme smallness of the neutrino Poincaré masses m_ν , resulting in the negative effective mass squares directly related to the scale of the gravito-electroweak unification [13]. This relation allows us to evaluate the gravito-electroweak scale from the currently reported experimental values for negative mass squares.

On the other hand, for now these data come with the statistical and systematic errors comparable with the reported values [31]. It is possible that the reduction in systematic and statistical errors will lead to shifting experimental values for mass squares to the positive region. However, the relation of the modified by geometry mass square with a gravito-electroweak scale is generic and model-independent, and we can expect that a gravito-electroweak scale would be estimated from the mass square data of the refined future experiments with the value close, at least by the order of magnitude, to the value obtained from the current data, $M_{GeW} \sim 60 \text{ TeV}$.

The relation of a particle mass with the spacetime symmetry is required not only by the Higgs mechanism for a particle acquiring its mass via spontaneous symmetry breaking of a scalar field, but also by General Relativity, in which masses of regular objects with the de Sitter vacuum interiors are generically related to breaking of spacetime symmetry from the de Sitter group in their interiors [7].

Our above analysis of the spacetime origin of negative mass squares for neutrinos was based on the relation of their masses with spacetime symmetry dictated by the Higgs mechanism. Analysis of the annihilation reaction $e^+e^- \rightarrow \gamma\gamma(\gamma)$ requires also appealing to the GR aspect of the mass–spacetime relation, since the experimental results suggest involvement of possible internal structure of particles participating in the reaction [15], while the Higgs mechanism provides the involvement of the de Sitter vacuum in their internal structure required for GR mass–spacetime relation [1,7].

The key point is that the minimal length $l_e = 1.57 \times 10^{-17}$ revealed in the experiments with the 5σ significance is much less than characteristic length scales for a particle, the classical electron radius $r_e = e^2/(m_e c^2) = 2.8 \times 10^{-13}$ cm and its Compton wavelength $\lambda_e = \hbar/(m_e c) = 3.9 \times 10^{-11}$ cm. Therefore, analysis of this reaction requires some model of an extended particle. Moreover, in this case the predictions of the applied techniques of QED- α^3 (based on the concept of a point-like dressed particle) contradict to the experimental results. Among a lot of models for an extended electron proposed during more than hundred years after its discovery by Sir Joseph John Thomson in 1897, the model presented by the Nonlinear Electrodynamics coupled to Gravity, seems to be most general. The NED-GR equations admit the class of regular solutions, which describe electrically charged spinning solitons. In the case of the purely electromagnetic reaction $e^+e^- \rightarrow \gamma\gamma(\gamma)$, the basic generic features predicted by the NED-GR dynamical equations for all regular electrically charged spinning objects provide certain general information about the origin of the minimal length in this reaction, so that a particular detailed modeling of particles internal structure is not needed.

The basic ingredient of electromagnetic solitons with the positive energy density is the de Sitter vacuum disk in their deep interiors. Asymptotic solutions for electromagnetic fields in the interior region determine the behavior of fields on the disk, and the stress–energy tensor calculated with these

asymptotic solutions, determines the equation of state and generates the geometry in the self-consistent and model-independent way. The basic generic features of the NED-GR electromagnetic solitons, found for an arbitrary gauge invariant electromagnetic lagrangian, suggest and allow us to explain the existence of a certain minimal length in the purely electromagnetic reaction of the electron-positron annihilation, as the characteristic length at which the electromagnetic attraction is balanced by the repulsive gravity of the de Sitter vacuum.

Another case involving the Higgs mechanism concerns heavy DM candidates with the interior de Sitter vacuum of the GUT scale: regular black hole remnants and G-lumps arising at the early stage of the universe evolution from the primordial fluctuations, and graviatoms formed by capturing available charged particles (for a detailed analysis, see [95]; for a review, see [25]). Their predicted observational signatures include the electromagnetic radiation with the frequency directly dependent on the de Sitter vacuum scale, and the induced proton decay in an underground detector, such as IceCUBE, due to the non-conservation of the baryon and lepton numbers in the GUT scale false vacuum interiors [26] (for a review, see [25]). This observational signature is challenging in the context of the Higgs mechanism also due to that predicted in supergravity unified models sensitivity of the proton lifetime to the Higgs boson mass [27].

Funding: This research received no external funding.

Conflicts of Interest: The author declares no conflict of interest.

References

1. Dymnikova, I. Mass, Spacetime Symmetry, de Sitter Vacuum, and the Higgs Mechanism. *Symmetry* **2020**, *12*, 634. [\[CrossRef\]](#)
2. Nishimura, K. Principles for a unified picture of fermions. *Progress Theor. Experim. Phys.* **2013**, *2013*, 023B06. [\[CrossRef\]](#)
3. Nishimura, K. Higgs-like mechanism for spontaneous spacetime symmetry breaking. *Phys. Rev. D* **2015**, *92*, 076010. [\[CrossRef\]](#)
4. Liu, J.C.H.; Wang, Y. Dark Energy from Ratio Gravity. *Phys. Rev. D* **2018**, *98*, 084060. [\[CrossRef\]](#)
5. Liu, J.C.H. A quantum theory of spacetime in spinor formalism and the physical reality of cross-ratio representation: The equation of density parameters of dark energy, matter, and ordinary matter is derived: $\Omega M^2 = 4\Omega b\Omega\Lambda$. *ScienceOpen Res.* **2016**. [\[CrossRef\]](#)
6. Liu, J.C.H. Quantization of ratio gravity in Minkowski spacetime and mass generation mechanism. *arXiv* **2019**, arXiv:1901.01845.
7. Dymnikova, I. The cosmological term as a source of mass. *Class. Quant. Grav.* **2002**, *19*, 725–740. [\[CrossRef\]](#)
8. Robertson, R.G.H.; Bowles, T.J.; Stephenson, G.J., Jr.; Wark, D.L.; Wilkerson, J.F.; Knapp, D.A. Limit on $\bar{\nu}_e$ mass from observation of the β decay of molecular tritium. *Phys. Rev. Lett.* **1991**, *67*, 957–959. [\[CrossRef\]](#)
9. Chang, T.; Ni, G. Explanation on Negative Mass-Square of Neutrinos. *arXiv* **2000**, arXiv:hep-ph/0009291v3.
10. Ingraham, R.L.; Luna-Acosta, G.A.; Wilkes, J.M. An explanation of the “negative neutrino mass squared” anomaly in tritium β -decay based on a theory of mass. *arXiv* **2001**, arXiv:hep-ph/0012060v1.
11. McKellar, B.H.J.; Garbutt, M.; Stephenson, G.J., Jr.; Goldman, T.; He, X.-G. Implications of results of neutrino mass experiments. *APPC* **2000**, *2001*, 12–17.
12. Ahluwalia, D.V.; Dymnikova, I. Spacetime as origin of neutrino oscillations. *Int. J. Mod. Phys. D* **2003**, *12*, 1787–1794
13. Ahluwalia, D.V.; Dymnikova, I. A theoretical case for negative mass-square for sub-ev particles. *Int. J. Mod. Phys. D* **2003**, *12*, 1787–1794. [\[CrossRef\]](#)
14. Dymnikova, I.; Sakharov, A.; Ulbricht, J. Minimal Length Scale in Annihilation. *arXiv* **2009**, arXiv:0907.0629.
15. Dymnikova, I.; Sakharov, A.; Ulbricht, J. Appearance of a minimal length in e^+e^- annihilation. *Adv. High Energy Phys.* **2014**, *2014*, 707812. [\[CrossRef\]](#)
16. Dymnikova, I. Spinning superconducting electrovacuum soliton. *Phys. Lett. B Part. Phys. Nucl. Phys. Cosmol.* **2006**, *639*, 368–372. [\[CrossRef\]](#)

17. Dymnikova, I.; Galaktionov, E. Regular rotating electrically charged black holes and solitons in nonlinear electrodynamics minimally coupled to gravity. *Class. Quant. Grav.* **2015**, *32*, 165015. [[CrossRef](#)]
18. Dymnikova, I.; Galaktionov, E. Basic Generic Properties of Regular Rotating Black Holes and Solitons. *Adv. Math. Phys.* **2017**, *2017*, 1035381. [[CrossRef](#)]
19. Coleman, S. Classical lumps and their quantum descendants. In *New Phenomena in Subnuclear Physics*; Zichichi, A., Ed.; Plenum Press: New York, NY, USA; London, UK, 1977; Volume 297.
20. Dymnikova, I. De Sitter-Schwarzschild black hole: Its particlelike core and thermodynamical properties. *Int. J. Mod. Phys. D* **1996**, *5*, 529–540. [[CrossRef](#)]
21. Kerr, R.P.; Schild, A. Some algebraically degenerate solutions of Einsteins gravitational field equations. *Proc. Symp. Appl. Math.* **1965**, *17*, 199.
22. Dymnikova, I. The algebraic structure of a cosmological term in spherically symmetric solutions. *Phys. Lett. B* **2000**, *472*, 33–38. [[CrossRef](#)]
23. Bronnikov, K.A.; Dymnikova, I.; Galaktionov, E. Multihorizon spherically symmetric spacetimes with several scales of vacuum energy. *Class. Quant. Grav.* **2012**, *29*, 095025–095047. [[CrossRef](#)]
24. Dymnikova, I. Generic Features of Thermodynamics of Horizons in Regular Spherical Space-Times of the Kerr-Schild Class. *Universe* **2018**, *4*, 63. [[CrossRef](#)]
25. Dymnikova, I. Dark Matter Candidates with Dark Energy Interiors Determined by Energy Conditions. *Symmetry* **2020**, *12*, 662. [[CrossRef](#)]
26. Dymnikova, I.; Khlopov, M. Regular black hole remnants and graviatoms with de Sitter interior as heavy dark matter candidates probing inhomogeneity of the early universe. *Int. J. Mod. Phys. D* **2015**, *24*, 1545002. [[CrossRef](#)]
27. Liu, M.; Nath, P. Higgs boson mass, proton decay, naturalness, and constraints of the LHC and Planck data. *Phys. Rev. D* **2013**, *87*, 095012. [[CrossRef](#)]
28. Montanet, L.; Porter, F.C.; Aguilar-Benitez, M.; Montanet, L.; Walck, C.; Crawford, R.L.; Kelly, R.L.; Rittenberg, A.; Trippe, T.G.; Wohl, C.G.; et al. Review of particle properties by particle data group. *Phys. Rev. D* **1994**, *50*, 1173–1823. [[CrossRef](#)]
29. Stoeffl, W.; Decman, D.J. Anomalous Structure in the Beta Decay of Gaseous Molecular Tritium. *Phys. Rev. Lett.* **1995**, *75*, 3237. [[CrossRef](#)]
30. Bilenky, S.M. Neutrinos: Majorana or Dirac? *Universe* **2020**, *6*, 134. [[CrossRef](#)]
31. Aker, M.; Altenmüller, K.; Arenz, M. ((KATRIN Collaboration). Improved Upper Limit on the Neutrino Mass from a Direct Kinematic Method by KATRIN. *Phys. Rev. Lett.* **2019**, *123*, 221802. [[CrossRef](#)]
32. Huang, G.; Rodejohann, W.; Zhou, S. Effective neutrino masses in KATRIN and future tritium beta-decay experiments. *Phys. Rev. D* **2020**, *101*, 016003. [[CrossRef](#)]
33. Pakvasa S.; Valle, J.W. Neutrino Properties Before and After KamLAND. *Proc. Indian Natl. Sci. Acad.* **2004**, *70A*, 189–222.
34. Otten, E.W.; Weinheimer, C. Neutrino mass limit from tritium β -decay. *Rept. Prog. Phys.* **2008**, *71*, 086201. [[CrossRef](#)]
35. Gürsey, F. Group theoretical concepts and methods in elementary particle physics. In *Group Theoretical Concepts and Methods in Elementary Particle Physics: Lectures of the Istanbul Summer School in Theoretical Physics*; Gürsey, F., Ed.; Gordon and Breach: New York, NY, USA, 1964.
36. Ryder, L.H. *Quantum Field Theory*; Cambridge University Press: Cambridge, UK, 1987.
37. Antoniadis, I. A possible new dimension at a few TeV. *Phys. Lett. B* **1990**, *246*, 377–384. [[CrossRef](#)]
38. Arkani-Hamed, N.; Dimopoulos, S.; Dvali, G.; Kaloper, N. Infinitely large new new dimensions. *Phys. Rev. Lett.* **2000**, *84*, 586–589. [[CrossRef](#)]
39. Dvali, G.; Smirnov, A.Y. Probing large extra dimensions with neutrinos. *Nucl. Phys. B* **1999**, *563*, 63–81. [[CrossRef](#)]
40. Dirac, P.A.M. An extensible model of the electron. *Proc. R. Soc. Lond. A* **1962**, *268*, 57–67.
41. Dymnikova, I. Regular electrically charged vacuum structures with de Sitter center in nonlinear electrodynamics coupled to general relativity. *Class. Quant. Grav.* **2004**, *21*, 4417–4428. [[CrossRef](#)]
42. Gürses, M.; Gürsey, F. Lorentz covariant treatment of the Kerr-Schild geometry. *J. Math. Phys.* **1975**, *16*, 2385–2391. [[CrossRef](#)]
43. Newman, E.T.; Janis, A.J. Note on the Kerr Spinning Particle Metric. *J. Math. Phys.* **1965**, *6*, 915–917. [[CrossRef](#)]

44. Newman, E.T.; Cough, E.; Chinnapared, K.; Exton, A.; Prakash, A.; Torrence, R. Metric of a rotating charged mass. *J. Math. Phys.* **1965**, *6*, 918–919. [[CrossRef](#)]
45. Carter, B. Global structure of the Kerr family of gravitational fields. *Phys. Rev.* **1968**, *174*, 1559–1571. [[CrossRef](#)]
46. Dymnikova, I.; Galaktionov, E. Dynamics of Electromagnetic Fields and Structure of Regular Rotating Electrically Charged Black Holes and Solitons in Nonlinear Electrodynamics Minimally Coupled to Gravity. *Universe* **2019**, *5*, 205. [[CrossRef](#)]
47. Burinskii, A. Source of the Kerr–Newman solution as a supersymmetric domain-wall bubble: 50 years of the problem. *Phys. Lett. B* **2016**, *754*, 99–103. [[CrossRef](#)]
48. Burinskii, A. Supersymmetric bag model for unification of gravity with spinning particles. *Phys. Part. Nucl.* **2018**, *49*, 958. [[CrossRef](#)]
49. Pope, T.; Hofer, W. Spin in the extended electron model. *Front. Phys.* **2017**, *12*, 128503. [[CrossRef](#)]
50. Pope, T.; Hofer, W. An Extended Electron Approach to the General Many-Body Problem. *arXiv* **2018**, arXiv:1801.06242.
51. Burinskii, A. Features of spinning gravity in particle physics: Supersymmetric core of the Kerr–Newman electron. *J. Phys. Conf. Ser.* **2019**, *1275*, 012031. [[CrossRef](#)]
52. Israel, W. Source of the Kerr metric. *Phys. Rev. D* **1970**, *2*, 641–646. [[CrossRef](#)]
53. Chandrasekhar, S. *The Mathematical Theory of Black Holes*; Clarendon Press: Oxford, UK, 1983.
54. Ayon-Beato, E.; Garcia, A. Regular black hole in general relativity coupled to nonlinear electrodynamics. *Phys. Rev. Lett.* **1998**, *80*, 5056–5059. [[CrossRef](#)]
55. Ayon-Beato, E.; Garcia, A. New regular black hole solution from nonlinear electrodynamics. *Phys. Lett. B* **1999**, *464*, 25–29. [[CrossRef](#)]
56. Ayon-Beato, E.; Garcia, A. Non-singular charged black hole solution for non-linear source. *Gen. Relativ. Gravit.* **1999**, *31*, 629–633. [[CrossRef](#)]
57. Ayon-Beato, E.; Garcia, A. Four parametric regular black hole solution. *Gen. Relativ. Gravit.* **2005**, *37*, 635–641. [[CrossRef](#)]
58. Salazar, H.; Garcia, A.; Plebański, J. Duality rotations and type D solutions to Einstein equations with nonlinear electromagnetic sources. *J. Math. Phys.* **1987**, *28*, 2171–2181. [[CrossRef](#)]
59. Bronnikov, K.A. Regular magnetic black holes and monopoles from nonlinear electrodynamics. *Phys. Rev. D* **2001**, *63*, 044005. [[CrossRef](#)]
60. Dymnikova, I.; Galaktionov, E.; Tropp, E. Existence of electrically charged structures with regular center in nonlinear electrodynamics minimally coupled to gravity. *Adv. Math. Phys.* **2015**, *2015*, 496475. [[CrossRef](#)]
61. Tiomno, J. Electromagnetic field of rotating charged bodies. *Phys. Rev. D* **1973**, *7*, 992–997. [[CrossRef](#)]
62. Burinskii, A.; Hildebrandt, S.R. New type of regular black hole solutions from nonlinear electrodynamics. *Phys. Rev. D* **2002**, *65*, 104017. [[CrossRef](#)]
63. Dymnikova, I. Electromagnetic source for the Kerr–Newman geometry. *Intern. J. Mod. Phys. D* **2015**, *24*, 1550094. [[CrossRef](#)]
64. Landau, L.D.; Lifshitz, E.M. *Electrodynamics of Continued Media*; Pergamon Press: Oxford, UK, 1993.
65. Dymnikova, I. Origin of the magnetic momentum for regular electrically charged objects described by nonlinear electrodynamics coupled to gravity. *Intern. J. Mod. Phys. D* **2019**, *28*, 1950011. [[CrossRef](#)]
66. Quigg, C. *Gauge Theories of the Strong, Weak and Electromagnetic Interactions*; Addison-Wesley Publishing Company: Redwood City, CA, USA, 1983.
67. Dymnikova, I. Spherically symmetric space-time with the regular de Sitter center. *Int. J. Mod. Phys. D* **2003**, *12*, 1015–1034. [[CrossRef](#)]
68. Poisson, E.; Israel, W. Structure of the black hole nucleus. *Class. Quant. Grav.* **1988**, *5*, L201–L205. [[CrossRef](#)]
69. Frolov, V.P.; Markov, M.A.; Mukhanov, V.F. Black holes as possible sources of closed and semiclosed worlds. *Phys. Rev. D* **1990**, *41*, 383–394. [[CrossRef](#)] [[PubMed](#)]
70. Dymnikova, I. Vacuum nonsingular black hole. *Gen. Relativ. Gravit.* **1992**, *24*, 235–242. [[CrossRef](#)]
71. Dymnikova, I. Internal structure of nonsingular spherical black holes. In *Internal Structure of Black Holes and Spacetime Singularities*; Burko, M., Ori, A., Eds.; Bristol In-t of Physics Publishing: Bristol, UK; Philadelphia, PA, USA; Annals of the Israel Physical Society 13: Jerusalem, Israel, 1997; pp. 422–440.
72. Berej, W.; Matyjasek, J.; Tryniecki, D.; Woronowicz, M. Regular black holes in quadratic gravity. *Gen. Relativ. Gravit.* **2006**, *38*, 885–906. [[CrossRef](#)]

73. Bonanno, A.; Reuter, M. Spacetime structure of an evaporating black hole in quantum gravity. *Phys. Rev. D* **2006**, *73*, 083005–083017. [[CrossRef](#)]
74. Nicolini, P. Noncommutative black holes, the final appeal to quantum gravity: A review. *Int. J. Mod. Phys. A* **2009**, *24*, 1229–1308. [[CrossRef](#)]
75. Perez, A. Spin foam models for quantum gravity. *Class. Quant. Grav.* **2003**, *20*, R43–R104. [[CrossRef](#)]
76. Rovelli, C. *Quantum Gravity*; Cambridge University Press: Cambridge, UK, 2004.
77. Dymnikova, I. Dark energy and spacetime symmetry. *Universe* **2017**, *3*, 20. [[CrossRef](#)]
78. Bronnikov, K.A.; Dobosz, A.; Dymnikova, I. Nonsingular vacuum cosmologies with a variable cosmological term. *Class. Quant. Grav.* **2003**, *20*, 3797–3814. [[CrossRef](#)]
79. Dymnikova, I.; Soltysek, B. Spherically symmetric space-time with two cosmological constants. *Gen. Relativ. Grav.* **1998**, *30*, 1775–1793. [[CrossRef](#)]
80. Dymnikova, I. The fundamental roles of the de Sitter vacuum. *Universe* **2020**, *6*, 101. [[CrossRef](#)]
81. Caldwell, R.R. A phantom menace? Cosmological consequences of a dark energy component with super-negative equation of state. *Phys. Lett. B* **2002**, *545*, 23–29. [[CrossRef](#)]
82. Gibbons, G.W.; Hawking, S.W. Cosmological event horizons, thermodynamics, and particle creation. *Phys. Rev. D* **1977**, *15*, 2738–2751. [[CrossRef](#)]
83. Dymnikova, I.; Korpusik, M. Regular black hole remnants in de Sitter space. *Phys. Lett. B* **2010**, *685*, 12–18. [[CrossRef](#)]
84. Myung, Y.S.; Kim, Y.W.; Park, Y.J. Quantum Cooling Evaporation Process in Regular Black Holes. *Phys. Lett. B* **2007**, *656*, 221–225. [[CrossRef](#)]
85. Dymnikova, I.; Korpusik, M. Thermodynamics of Regular Cosmological Black Holes with the de Sitter Interior. *Entropy* **2011**, *13*, 1967–1991. [[CrossRef](#)]
86. Carballo-Rubio, R.; Di Filippo, F.; Liberati, S.; Pacilio, C.; Visser, M. On the viability of regular black holes. *JHEP* **2018**, *2018*, 23. [[CrossRef](#)]
87. MacGibbon, J.H. Can Planck-mass relics of evaporating black holes close the Universe? *Nature* **1987**, *329*, 308–309. [[CrossRef](#)]
88. Carr, B.J.; Gilbert, J.H.; Lidsey, J.E. Black hole relics and inflation: Limits on blue perturbation spectra. *Phys. Rev. D* **1994**, *50*, 4853–4867. [[CrossRef](#)]
89. Rovelli, C.; Vidotto, F. Small Black/White Hole Stability and Dark Matter. *Universe* **2018**, *4*, 127. [[CrossRef](#)]
90. Susskind, L. The World as a hologram. *J. Math. Phys.* **1995**, *36*, 6377–6396. [[CrossRef](#)]
91. Ellis, G.F.R. Astrophysical black holes may radiate, but they do not evaporate. *arXiv* **2013**, arXiv:1310.4771.
92. Dymnikova, I.; Galaktionov, E. Stability of a vacuum nonsingular black hole. *Class. Quant. Grav.* **2005**, *22*, 2331–2357. [[CrossRef](#)]
93. Dymnikova, I.; Galaktionov, E. Vacuum dark fluid. *Phys. Lett. B* **2007**, *645*, 358–364. [[CrossRef](#)]
94. Boyanovsky, D.; de Vega, H.J.; Schwarz, D.J. Phase transitions in the early and present universe. *Annu. Rev. Nucl. Part. Sci.* **2006**, *56*, 441–500. [[CrossRef](#)]
95. Dymnikova, I.; Fil’chenkov, M. Graviatoms with de Sitter interior. *Adv. High Energy Phys.* **2013**, *2013*, 746894. [[CrossRef](#)]
96. Kalashev, O.E.; Rubtsov, G.I.; Troitsky, S.V. Sensitivity of cosmic-ray experiments to ultrahigh-energy photons: Reconstruction of the spectrum and limits on the superheavy dark matter. *Phys. Rev. D* **2009**, *80*, 103006. [[CrossRef](#)]

Publisher’s Note: MDPI stays neutral with regard to jurisdictional claims in published maps and institutional affiliations.



© 2020 by the author. Licensee MDPI, Basel, Switzerland. This article is an open access article distributed under the terms and conditions of the Creative Commons Attribution (CC BY) license (<http://creativecommons.org/licenses/by/4.0/>).